ELSEVIER

Materials Science and Engineering A280 (2000) 263–269

MATERIALS SCIENCE & ENGINEERING A

www.elsevier.com/locate/msea

Particle size distribution and dislocation density determined by high resolution X-ray diffraction in nanocrystalline silicon nitride powders

J. Gubicza [a], J. Szépvölgyi [b], I. Mohai [b], L. Zsoldos [a], T. Ungár [a,*]

[a] *Department of General Physics, Eötvös University, PO Box 32, Budapest H-1518, Hungary*
[b] *Research Laboratory of Materials and Environmental Chemistry, Chemical Research Center, Hungarian Academy of Sciences, Pusztaszeri út 59–67, Budapest H-1025, Hungary*

Received 7 July 1999; received in revised form 8 October 1999

Abstract

Two silicon nitride powders were investigated by high resolution X-ray diffraction. The first sample was crystallized from the powder prepared by the vapour phase reaction of silicon tetrachloride and ammonia while the second was a commercial powder produced by the direct nitridation of silicon. Their particle size and dislocation density were obtained by the recently developed modified Williamson–Hall and Warren–Averbach procedures from X-ray diffraction profiles. Assuming that the particle size distribution is log-normal the size distribution function was calculated from the size parameters derived from X-ray diffraction profiles. The size distributions determined from TEM micrographs were in good correlation with the X-ray results. The area-weighted average particle size calculated from nitrogen adsorption isotherms was in good agreement with that obtained from X-rays. The powder produced by silicon nitridation has a wider size distribution with a smaller average size than the powder prepared by vapour phase reaction. The dislocation densities were found to be between about 10^{14} and 10^{15} m^{-2}. Published by Elsevier Science S.A. All rights reserved.

Keywords: X-ray line profile analysis; Nanocrystalline silicon nitride; Particle size distribution; Dislocation density

1. Introduction

Dense silicon nitride ceramics are important structural materials because of their good room and high temperature mechanical properties. Silicon nitride ceramics of low porosity are usually densified by liquid-phase sintering [1]. Consequently, the average particle size and the particle size distribution have a great influence on the density, the phase composition and the microstructure, and therefore on the mechanical properties of the resulting ceramics [2–4]. Cambier et al. have found that the density of the specimen at the beginning of sintering is larger if the particle size distribution of the starting powder is wider [4]. It has been also established that during sintering the densification depends mainly on the inverse of the average particle size. On the other hand, if the particle size distribution at the beginning is wide then coarsening of the particles can occur leading to lower sinterability as densification proceeds [4].

The particle size of silicon nitride powder can be measured by transmission electron microscopy (TEM), however this is a laborious and time consuming procedure. Furthermore, the volume that one can examine in a microscope is always very small in comparison with the entire sample leading to uncertainty as to whether a truly characteristic region of the sample was investigated. On the other hand, X-ray diffraction examines a much larger fraction of the specimen, and the preparation of the sample and the evaluation of the measurements are not so laborious. Krill and Birringer have recently developed a procedure to determine size distribution from the Fourier transform of X-ray diffraction profiles [5]. In this procedure, however, the anisotropic strain broadening has not been accounted for and only

* Corresponding author. Tel.: +36-1-3722801; fax: +36-1-372-2811.
E-mail address: ungar@ludens.elte.hu (T. Ungár)

0921-5093/00/$ - see front matter Published by Elsevier Science S.A. All rights reserved.
PII: S0921-5093(99)00702-9

the Fourier coefficients of diffraction profiles were used. It has been shown recently that strain anisotropy can be well accounted for by the dislocation model of the mean square strain [6–12]. The model described in these papers takes into account that the contrast caused by dislocations depends on the relative directions of the line and Burgers vectors of the dislocations and the diffraction vector, respectively. Anisotropic contrast can thus be summarised in contrast factors, C, which can be calculated numerically on the basis of the crystallography of dislocations and the elastic constants of the crystal [8–12]. By appropriate determination of the type of dislocations and Burgers vectors present in the crystal, the average contrast factors, C, for the different Bragg reflections can be determined. Using the average contrast factors in the modified Williamson–Hall plot and in the modified Warren–Averbach procedure, the different averages of particle sizes and the dislocation density can be obtained [6,7]. It has also been shown that the volume-weighted and the area-weighted average particle sizes determined from the integral breadths and the Fourier coefficients of the diffraction profiles, respectively, can be used for the determination of particle size distributions [5].

The aim of the present paper is

1. to compare the particle size distribution and the dislocation density in two silicon nitride powders produced by essentially different methods of synthesis and
2. to investigate the correlation between the particle size distribution determined by TEM measurements, the area-weighted average particle size calculated from the specific surface area and those obtained by X-ray diffraction line profile analysis.

2. Experimental details

2.1. Powder preparation

Two kinds of silicon nitride powders were investigated. The first one (SN1500) was a laboratory produced powder synthesized by the vapour-phase reaction of silicon tetrachloride and ammonia in a radiofrequency thermal plasma reactor under conditions given previously [13,14]. The as-synthesized powder was subjected to a two-step thermal processing to remove NH_4Cl and $Si(NH)_2$ by-products formed due to the NH_3 excess in the plasma synthesis. The powder was treated in nitrogen at 400°C for 1 h and subsequently at 1100°C for 1 h to achieve the complete decomposition of by-products. This resulting powder was predominantly amorphous with a crystalline content of about 20 vol.%. The crystallization procedure was performed in a horizontal laboratory furnace in flowing nitrogen at 0.1 MPa, at annealing temperature of 1500°C for 2 h. After crystallization the crystalline content of the powder was about 80 vol.%. The second powder was a commercial one produced by nitridation of silicon and post-milling (LC12, Starck, Germany).

2.2. X-ray diffraction technique

The crystalline phases were identified by X-ray diffraction (XRD) using a Guinier–Hagg focusing camera and $CuK\alpha_1$ radiation. The relative amounts of α- and β-Si_3N_4 phases were determined from the XRD pattern using the Gazzara and Messier method [15]. In this procedure the intensities of the 201, 102 and 210 reflections of α-Si_3N_4 and the 200, 101 and 210 reflections of β-Si_3N_4 were averaged to minimize preferred orientation effects and statistical errors. The ratio of the amounts of α- and β-Si_3N_4 phases was calculated from these averaged intensities using the formula proposed by Camuscu et al. [16].

The diffraction profiles were measured by a special double crystal diffractometer with negligible instrumental broadening [6,17]. A fine focus rotating cobalt anode (Nonius FR 591) was operated as a line focus at 36 kV and 50 mA ($\lambda = 0.1789$ nm). The symmetrical 220 reflection of a Ge monochromator was used in order to have wavelength compensation at the position of the detector. The $K\alpha_2$ component of the Co radiation was eliminated by an 0.16 mm slit between the source and the Ge crystal. By curving the Ge crystal sagittally in the plane perpendicular to the plane-of-incidence the brilliance of the diffractometer was increased by a factor of three. The profiles were registered by a linear position sensitive gas flow detector, OED 50 Braun, Munich. In order to avoid air scattering and absorption the distance between the specimen and the detector was overbridged by an evacuated tube closed by mylar windows.

TEM (JEOL JEM200CX) has been used for direct measurement of the particle size and size distribution. Bright field images of the particles were used to measure the particle size in both powder samples.

The specific surface areas of the powders were determined from the nitrogen adsorption isotherms by the BET (Brunauer–Emmett–Teller) method [18]. Assuming that the particles have spherical shape, the area-weighted average particle size (t) in nm was calculated as $t = 6000/qS$ where q is the density in g cm^{-3} and S is the specific surface area in m^2 g^{-1}.

3. Evaluation of the X-ray diffraction profiles

3.1. The modified Williamson–Hall and Warren–Averbach methods

Assuming that strain broadening is caused by dislo-

cations the full widths at half maximum (FWHM) of diffraction profiles can be given by the modified Williamson–Hall plot as [6,7]:

$$\Delta K = \gamma/D + \alpha(K\bar{C}^{1/2}) + O(K^2\bar{C}), \quad (1)$$

where D is a size parameter characterising the column lengths in the specimen, γ equals to 0.9, α is a constant depending on the effective outer cut-off radius, the Burgers vector and the density of dislocations, C is the contrast factor of dislocations depending on the relative positions of the diffraction vector and the Burgers and line vectors of the dislocations and on the character of dislocations [6,8–12] and O stands for higher order terms in $K\bar{C}^{1/2}$. K is the length of the diffraction vector: $K = 2 \sin\theta/\lambda$, where θ is the diffraction angle and λ is the wavelength of X-rays. $\Delta K = \cos\theta[\Delta(2\theta)]/\lambda$, where $\Delta(2\theta)$ is the FWHM of the diffraction peak. The size parameter corresponding to the FWHM, D, is obtained from the intercept at $K = 0$ of a smooth curve according Eq. (1) [6]. The modified Williamson–Hall procedure was also applied for the integral breadths of the profiles. In this case γ was taken as 1 and the obtained size parameter denoted by d gives the volume-weighted average column length in the sample [19]. We note that in the present case shape isotropy is assumed which holds to a great extent as supported by TEM observations.

$\bar{C}$ is the weighted average of the individual C factors over the dislocation population in the crystal. In the present case the C factors could not be calculated directly since, to the knowledge of the authors, the anisotropic elastic constants of Si_3N_4 are not available. Therefore the average $\bar{C}$ factors were determined by the following indirect method. Based on the theory of line broadening caused by dislocations it has been shown that the average dislocation contrast factor in an untextured hexagonal polycrystalline specimen is the following function of the invariants of the fourth order polynomials of Miller indices hkl [20]:

$$\bar{C} = \bar{C}_{hk0}\left[1 + \frac{[A(h^2+k^2+(h+k)^2) + Bl^2]l^2}{\left[h^2+k^2+(h+k)^2+\frac{3}{2}\left(\frac{a}{c}\right)^2 l^2\right]^2}\right], \quad (2)$$

where $\bar{C}_{hk0}$ is the average dislocation contrast factor for the $hk0$ reflections, A and B are parameters depending on the elastic constants and on the character of dislocations in the crystal and c/a is the ratio of the two lattice constants of the hexagonal crystal ($c/a = 0.7150$ and 0.3826 for α- and β-Si_3N_4, respectively [21]). Inserting Eq. (2) into Eq. (1) the latter one was solved for D, α, A and B by the method of least squares. As $\bar{C}_{hk0}^{1/2}$ is a multiplier of K in Eq. (1), its value can not be determined by this method. The value of $\bar{C}_{hk0}$ was calculated numerically assuming elastic isotropy because of the lack of the knowledge of anisotropic elastic constants. The isotropic $\bar{C}_{hk0}$ factor was evaluated for the most commonly observed dislocation slip system in silicon nitride [21]: $\langle 0001\rangle\{1010\}$. Taking 0.24 as the value of the Poisson's ratio [22] $\bar{C}_{hk0} = 0.0279$ was obtained for both α- and β-Si_3N_4.

The modified Warren–Averbach equation is [6]:

$$\ln A(L) \cong \ln A^S(L) - \rho B L^2 \ln(R_e/L)(K^2\bar{C}) + O(K^4\bar{C}^2), \quad (3)$$

where $A(L)$ is the real part of the Fourier coefficients of the diffraction profiles, A^S is the size Fourier coefficient as defined by Warren [23], ρ is the dislocation density, $B = \pi b^2/2$ (b is the length of the Burgers vector), R_e is the effective outer cut-off radius of dislocations and O stands for higher order terms in $K^2\bar{C}$. L is the Fourier length defined as [23]:

$$L = na_3, \quad (4)$$

where $a_3 = \lambda/2(\sin\theta_2 - \sin\theta_1)$, n are integers starting from 0, λ is the wavelength of X-rays and $(\theta_2 - \theta_1)$ is the angular range of the measured diffraction profile. The average dislocation contrast factors C determined from the modified Williamson–Hall plot of FWHM were also used in Eq. (3). The size parameter corresponding to the Fourier coefficients is denoted by L_0. It is obtained from the size Fourier coefficients, A^S, by taking the intercept of the initial slope at $A^S = 0$ [23] and it gives the area-weighted average column length [19].

3.2. Determination of the average particle size and the particle size-distribution from X-ray diffraction

Three size parameters were determined by the modified Williamson–Hall and Warren–Averbach procedures: D from the FWHM, d from the integral breadths and L_0 from the Fourier coefficients. It can be shown that d and L_0 are the volume- and the area-weighted average column length in the specimen [19]. For spherical particles the volume-weighted and the area-weighted average particle sizes, $\langle x\rangle_{vol}$ and $\langle x\rangle_{area}$, can be calculated from the volume and the area-weighted average column lengths, respectively, as follows: $\langle x\rangle_{vol} = 4d/3$ and $\langle x\rangle_{area} = 3L_0/2$ [5,24,25]. These two independent weighted averages of particle size can be used for the determination of particle size distribution if it is approximated by a known function having two free parameters. It was observed by many authors that the particle size distribution of nanocrystalline materials is log-normal [5,26,27]:

$$f(x) = \frac{1}{\sqrt{2\pi}\ln\sigma}\frac{1}{x}\exp\left\{-\frac{[\ln(x/m)]^2}{2\ln^2\sigma}\right\}, \quad (5)$$

where x is the particle size, σ is the variance and m is the median of the size distribution function $f(x)$. The

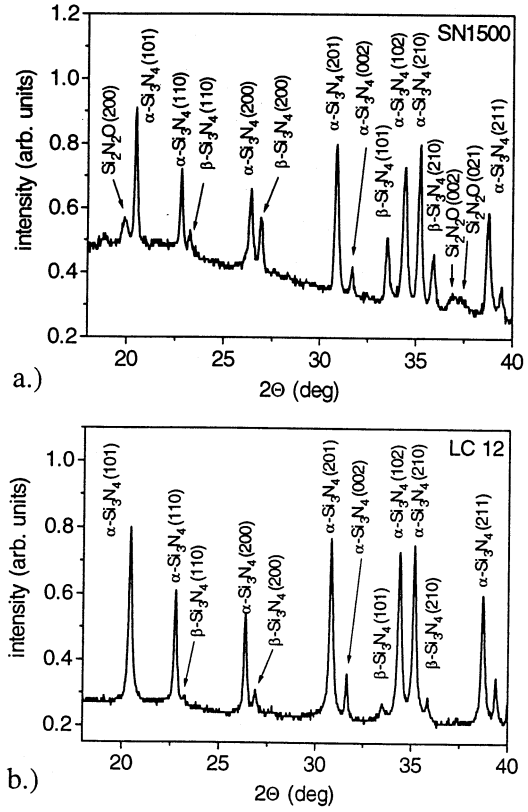

Fig. 1. X-ray diffractograms of the powders produced (a) by vapor-phase synthesis in thermal plasma followed by crystallization (SN1500) and (b) by silicon nitridation and postmilling (LC12).

Table 1
The values of the parameters $\overline{C}_{hk0}$, A and B used for the calculation of the average dislocation contrast factors for α- and β-Si_3N_4 in powder SN1500 and for α-Si_3N_4 in sample LC12

		$\overline{C}_{hk0}$	A	B
SN1500	α-Si3N4	0.0279	3.271	−1.673
	β-Si3N4	0.0279	−28.52	44.89
LC12	α-Si3N4	0.0279	3.329	−1.778

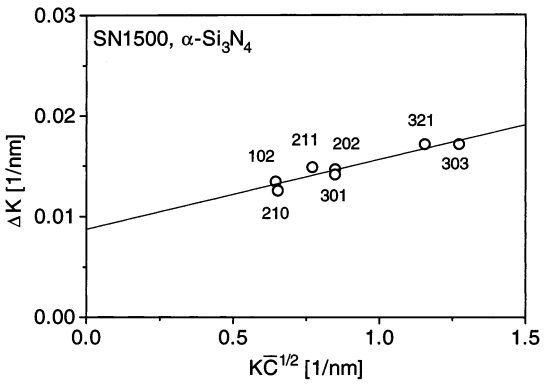

Fig. 2. The FWHM as a function of $K\overline{C}^{1/2}$ for α-Si_3N_4 in powder SN1500, the modified Williamson–Hall plot according to Eq. (1). The numbers at the symbols represent the Miller indices.

parameters σ and m for a log-normal distribution are given in terms of the average particle sizes [28]:

$$\sigma = \exp\left[\left(\ln\frac{\langle x\rangle_{vol}}{\langle x\rangle_{area}}\right)^{0.5}\right], \quad (6a)$$

$$m = (\langle x\rangle_{vol})^{-2.5}(\langle x\rangle_{area})^{3.5}. \quad (6b)$$

Using these expressions, σ and m were calculated for the two silicon nitride powders.

4. Results and discussion

Fig. 1 shows the X-ray diffractograms of the two powders. The X-ray phase analysis shows that in both powders the major phase is α-Si_3N_4. Beside this phase β-Si_3N_4 was also identified in the powders. The mass ratios of α- to β-Si_3N_4 were 5.1 and 13.4 for samples SN1500 and LC12, respectively. A small amount of Si_2N_2O was also found in powder SN1500. The Si_2N_2O phase in powder SN1500 and β-Si_3N_4 in material LC12 will be neglected in the following calculations because of their small amounts compared with α-Si_3N_4.

The values of $\overline{C}_{hk0}$, A and B were calculated by the method described in Section 3.1 for α- and β-Si_3N_4 in powder SN1500 and for α-Si_3N_4 in sample LC12, and are listed in Table 1. The modified Williamson–Hall plots of the FWHM and the integral breadth for α-Si_3N_4 phase in powder SN1500 according to Eq. (1) are shown in Figs. 2 and 3, respectively. The linear regressions to the FWHM and the integral breadth give $D = 103$ nm and $d = 91$ nm, respectively. The results obtained from similar procedures for β-Si_3N_4 in powder SN1500 and α-Si_3N_4 in material LC12 are listed in Table 2.

A typical plot according to the modified Warren–Averbach procedure given in Eq. (3) is shown in Fig. 4 for α-Si_3N_4 in sample SN1500. From the quadratic regressions the particle size coefficients, A^S were determined. The intersections of the initial slopes at $A^S(L) = 0$ yield the area-weighted average column length: $L_0 = 62$ and 57 for α-Si_3N_4 and β-Si_3N_4 in powder SN1500, respectively, and 41 nm for α-Si_3N_4 in sample LC12 (see also Table 2). It can be seen that in the sample produced by vapour-phase reaction (SN1500) the weighted average column lengths of α-Si_3N_4 agree with those of β-Si_3N_4 within experimental error, therefore the average particle sizes calculated for the major α-Si_3N_4 phase were taken as characteristic parameters for sample SN1500. The volume- and the area-weighted average particle sizes calculated from the average column lengths for α-Si_3N_4 in powders SN1500 and LC12 are shown in Table 2. It can be also established that the average column lengths and particle sizes for α-Si_3N_4 in powder prepared by silicon nitridation (LC12) are significantly lower than those for sample SN1500.

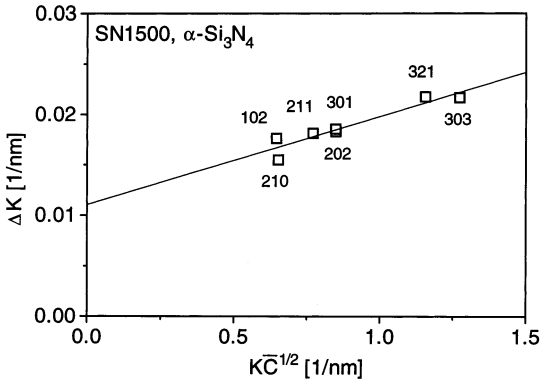

Fig. 3. The integral breadth as a function of $K\overline{C}^{1/2}$ for α-Si_3N_4 in powder SN1500, the modified Williamson–Hall plot according to Eq. (1). The numbers at the symbols represent the Miller indices.

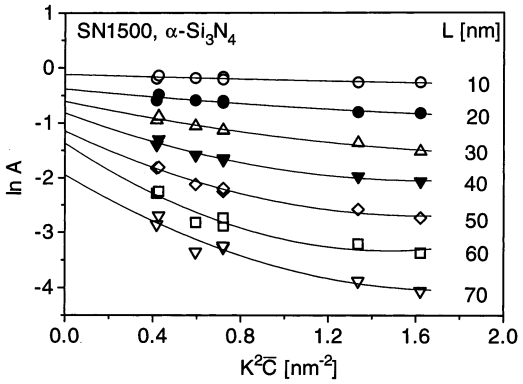

Fig. 4. The logarithm of the real part of the Fourier coefficients versus $K^2\overline{C}$, for α-Si_3N_4 in powder SN1500, the modified Warren–Averbach plot according to Eq. (3).

Log-normal particle size distribution functions were determined for the major α-Si_3N_4 phase in powders SN1500 and LC12 by the procedure described in Section 3.2. As the result of this calculation the two parameters, σ and m corresponding to the log-normal size distribution are obtained and listed in Table 2. The log-normal size-distribution functions, $f(x)$, corresponding to the σ and m values are shown as solid lines in Fig. 5a and b for powders SN1500 and LC12, respectively. The size distributions obtained from the TEM micrographs are shown as bar-graphs in Fig. 5a and b. (The scales of the bar-diagrams and the size-distribution functions are on the left- and the right hand side of the figures.) In the TEM measurements 300 particles were chosen at random in different areas in each powder. A typical TEM micrograph of powder LC12 is shown in Fig. 6. It can be established that the powder produced by silicon nitridation and milling (LC12) has lower value of m and higher σ than the powder synthesized by vapour phase reaction. This observation is supported by TEM results (see Fig. 5). The agreement between the bar-diagrams and the size-distribution functions is good for both samples. The small quantitative difference between the X-ray and the TEM results is probably due to the fact that the bar-diagram was obtained from a relatively small number of grains and that in the size distribution functions obtained by X-rays only the particles of the major α-Si_3N_4 phase were taken into account. To increase the number of grains for counting in TEM micrographs would need formidably greater efforts. About five orders of magnitude more grains contribute to the X-ray measurements. The good qualitative and quantitative agreement between the TEM and X-ray determined size distributions indicates that

1. the size distribution is log-normal in accordance with observations by other authors in many nanocrystalline materials [5,26,27]and,
2. the X-ray procedure described in Section 3.2 yields the size distribution in good agreement with direct observations.

The t value calculated from the specific surface area determined by BET method is given in Table 2. It can be seen that for both powders this value agrees well with the $\langle x \rangle_{area}$ determined from X-rays. It should be mentioned, however, that within the present experimental conditions only those particles or domains cause observable size broadening which are smaller than about 0.5 μm.

The dislocation density has been determined from the modified Warren–Averbach plot as follows [6,7]. The second coefficients in the quadratic regression to the Fourier coefficients provide the values of $\rho BL^2 \ln(R_e/L)$ as a function of L (see Eq. (3)). Plotting $\rho B \ln(R_e/L)$

Table 2
The values of the three size parameters D, d, L_0 determined from the FWHM, the integral breadth and the Fourier coefficients of the X-ray line profiles, respectively; the $\langle x \rangle_{vol}$ and the $\langle x \rangle_{area}$ average particle sizes obtained from X-rays; the two parameters characterizing the log-normal size distribution functions, σ and m; the t average particle size calculated from specific surface area; and the dislocation density (ρ) for α- and β-Si_3N_4 in powder SN1500 and for α-Si_3N_4 in sample LC12

		D (nm)	d (nm)	L_0 (nm)	$\langle x \rangle_{vol}$ (nm)	$\langle x \rangle_{area}$ (nm)	σ	m (nm)	t (nm)	ρ (m^{-2})
SN1500	α-Si_3N_4	103 ± 4	91 ± 4	62 ± 4	121	93	1.68	47	94	5.7×10^{14}
	β-Si_3N_4	99 ± 5	94 ± 4	57 ± 3						7.1×10^{15}
LC12	α-Si_3N_4	89 ± 5	66 ± 4	41 ± 3	88	62	1.82	25	71	7.7×10^{14}

versus ln L enables the graphic determination of ρ and R_e. The dislocation densities were obtained to be 5.7×10^{14} and 7.1×10^{15} m^{-2} for α-Si_3N_4 and β-Si_3N_4 in powder SN1500, respectively, and 7.7×10^{14} m^{-2} for α-Si_3N_4 in material LC12 (also listed in Table 2). As it can be seen there is no significant difference between the dislocation densities for α-Si_3N_4 in the powders produced by essentially different methods. However, β-Si_3N_4 in SN1500 sample has one order of magnitude higher dislocation density compared to α-Si_3N_4.

5. Conclusions

(1) It has been found that the silicon nitride powder produced by silicon nitridation and by post-milling had lower average particle size and wider size distribution than the sample obtained by crystallization of an amorphous thermal plasma silicon nitride powder.

(2) It has been established that the particle size distribution determined by X-ray line profile analysis agreed well with that obtained by direct TEM measurements for both silicon nitride powders.

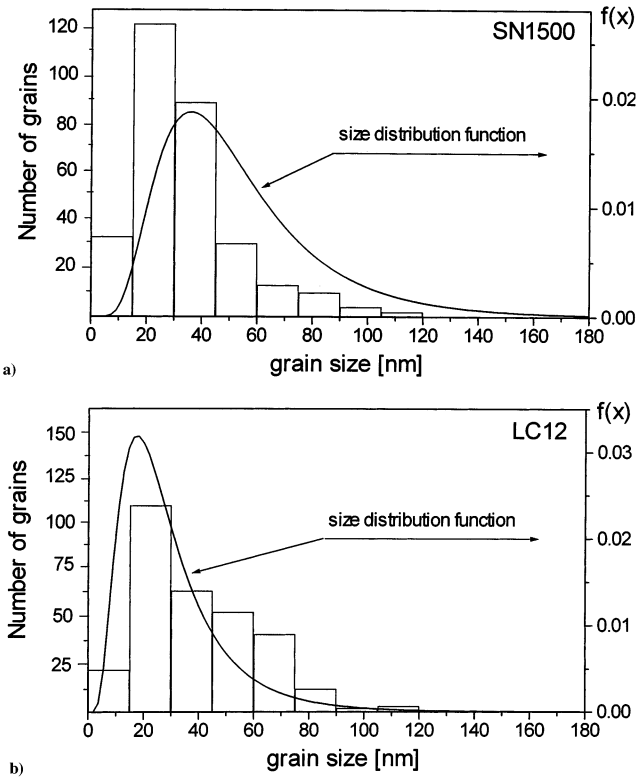

Fig. 5. Bar-diagrams of the size distributions obtained from TEM micrographs and the size distribution functions, $f(x)$ (solid lines), determined by X-rays for powders (a) SN1500 and (b) LC12, respectively.

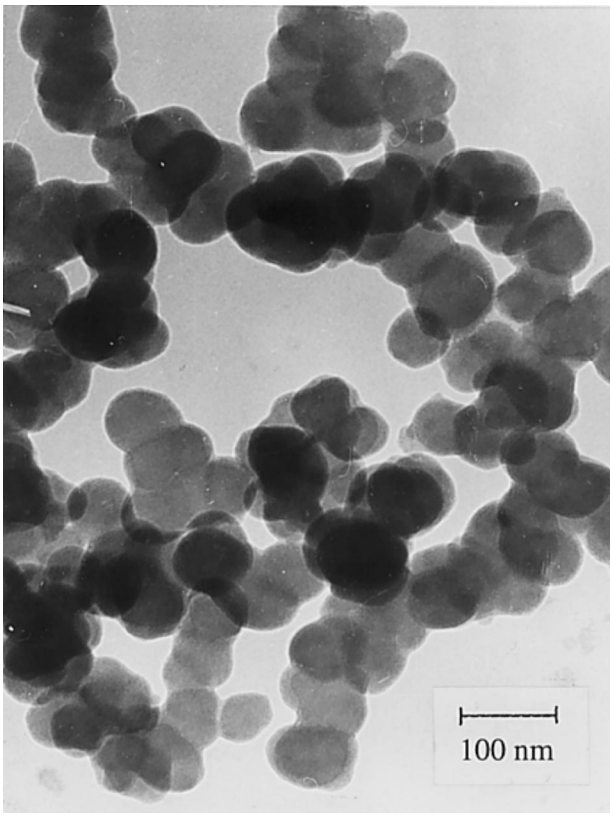

Fig. 6. TEM micrograph of powder LC12.

(3) The area-weighted average particle size obtained by X-rays is in good agreement with that calculated from specific surface area for both silicon nitride samples.

(4) No significant difference was found between the dislocation densities for α-Si_3N_4 in the powders produced by crystallization of an amorphous thermal plasma powder (5.7×10^{14} m^{-2}) and by nitridation of silicon and post-milling (7.7×10^{14} m^{-2}). At the same time β-Si_3N_4 in the sample crystallized after plasma synthesis had one order of magnitude higher dislocation density (7.1×10^{15} m^{-2}).

Acknowledgements

The authors are indebted to Dr Katalin Tasnady for the TEM measurements. The authors are especially grateful to Dr J. I. Langford for helpful discussions and comments on the interpretation of particle size and size distribution. Thanks are due to Gabor Ribarik for his kind assistance in the numerical fitting of the experimental data to Eqs. (1) and (2). The authors are grateful for the financial support of the Hungarian Scientific Research Fund, OTKA, Grant Nos. D-29339 and T029701 and the Hungarian Government Fund FKFP 0116/1997.

References

[1] G. Ziegler, J. Heinrich, G. Wotting, J. Mater. Sci. 22 (1987) 3041.
[2] G. Petzow, R. Sersale, Pure Appl. Chem. 59 (1987) 1674.
[3] J. Szépvölgyi, I. Mohai, in: G.N. Babini, et al. (Eds.), Engineering Ceramics '96: Higher Reliability through Processing, Kluwer Academic, Dordrecht, The Netherlands, 1997, p. 89.
[4] F. Cambier, A. Leriche, E. Gilbart, R.J. Brook, F.L. Riley, in: R. Freer (Ed.), The Physics and Chemistry of Carbides, Nitrides and Borides, Kluwer Academic, Dordrecht, The Netherlands, 1990, p. 13.
[5] C.E. Krill, R. Birringer, Phil. Mag. 77A (1998) 621.
[6] T. Ungár, A. Borbely, Appl. Phys. Lett. 69 (1996) 3173.
[7] T. Ungár, S. Ott, P. Sanders, A. Borbely, J.R. Weertman, Acta Mater. 46 (1998) 3693.
[8] T. Ungar, I. Dragomir, Á Révész, A. Borbély, J. Appl. Cryst. 32 (1999) 992.
[9] M. Wilkens, Phys. Stat. Sol. 104a (1987) K1.
[10] I. Groma, T. Ungar, M. Wilkens, J. Appl. Cryst. 21 (1988) 47.
[11] P. Klimanek, R. Kuzel Jr, J. Appl. Cryst. 21 (1988) 59.
[12] R. Kuzel Jr, P. Klimanek, J. Appl. Cryst. 21 (1988) 363.
[13] J. Szépvölgyi, I. Mohai, J. Mater. Chem. 5 (1995) 1227.
[14] J. Szépvölgyi, F.L. Riley, I. Mohai, I. Bertoti, E. Gilbart, J. Mater. Chem. 6 (1996) 1175.
[15] C.P. Gazzara, D.R. Messier, Ceram. Bull. 56 (1977) 777.
[16] N. Camuscu, D.P. Thompson, H. Mandal, J. Eur. Ceram. Soc. 17 (1997) 599.
[17] M. Wilkens, H. Eckert, Z. Naturforschung 19a (1964) 459.
[18] B.C. Lippenca, M.A. Hermanns, Powd. Met. 7 (1961) 66.
[19] A. Guinier, X-ray Diffraction, Freeman, San Francisco, CA, 1963.
[20] T. Ungár, G. Tichy, Phys. Stat. Sol. 171a (1999) 425.
[21] C.M. Wang, X. Pan, M. Ruehle, F.L. Riley, M. Mitomo, J. Mater. Sci. 31 (1996) 5281.
[22] K. Rajan, P. Sajgalik, J. Am. Ceram. Soc. 17 (1997) 1093.
[23] B.E. Warren, Progr. Metal Phys. 8 (1959) 147.
[24] M. Rand, J.I. Langford, J.S. Abell, Phil. Mag. B68 (1993) 17.
[25] A.J.C. Wilson, X-ray Optics, Methuen, London, 1962.
[26] C.D. Terwilliger, Y.M. Chiang, J. Am. Ceram Soc. 78 (1995) 2045.
[27] T. Ungar, A. Borbély, G.R. Goren-Muginstein, S. Berger, A.R. Rosen, Nanostruct. Mater. 11 (1999) 103.
[28] W.C. Hinds, Aerosol Technology: Properties, Behavior and Measurement of Airbone Particles, Wiley, New York, 1982.